

Improving Sound Wave Detection with Distributed Acoustic Sensing

Derrick Chambers, Peiyao Li & Jeffrey Shragge

*Center for Wave Phenomena and Dept. of Geophysics, Colorado School of Mines, Golden CO 80401
email: derrickchambers@mines.edu*

ABSTRACT

Over the past decade, the burgeoning field of distributed acoustic sensing (DAS) has greatly improved the quality and interpretability of many monitoring efforts and enabled new applications that were previously infeasible. One of the less-developed DAS research areas, especially for geophysical applications, is the recording of sound waves propagating in air. Here we detail our progressing work on quantifying and improving the ability of DAS systems to record sound waves, with the aim of deploying DAS acoustic sensors in heavy industrial settings. We record the DAS response to a suite of sources played by a small speaker for a fiber-optic cable deployed in several configurations: straight fiber laying on the ground, straight fiber suspended from the ceiling, loose fiber coils, a fiber-attached Plexiglas sheet, fiber wrapped around a tire, and fiber wrapped tightly around a PVC pipe. Although other studies have tested comparable configurations, we offer a relatively uniform comparison between each of the configurations. We find a straight cable (whether suspended or laying on the ground) does not record the source signal; however, the other configurations do with varying quality. The best overall recording system was produced by the cylinder with tightly wound fiber, though its sensitivity is suboptimal for frequencies less than 600 Hz. We conclude by discussing the next steps for this line of research.

Key words: DAS, Acoustics, Measurement, Acoustic Monitoring

1 INTRODUCTION

Distributed acoustic sensing (DAS) uses low-power, narrow-band lasers and naturally occurring impurities in fiber-optic cables to measure subtle dynamic strains along long cable segments. Although at any point along the sensing cable DAS has a much lower sensitivity than a comparable point sensor, its distributed nature and per-channel cost-effectiveness have made possible, or greatly improved, a wide range of distributed sensing applications. Some major focus areas include monitoring hydraulic fracturing (Molenaar and Cox, 2013) and associated microseismicity (Karrenbach et al., 2017), recording regional and global earthquakes (Lindsey et al., 2017), determining seismic site characteristics for earthquake hazard assessment (Spica et al., 2020), and many other applications (see Lindsey et al., 2020, for a review of geophysical DAS applications).

Although the bulk of DAS research focuses on recording vibrations transmitted through solid materials, some studies have explored the transmission of mechanical waves through underwater or atmospheric environments. For example, Zuo et al. (2021) characterized the signals transmitted via boat to lake-bed armored fiber cables as the first step in using ocean-bottom cables as receivers for underwater communication. Lior et al. (2021) used seafloor fiber cables for imaging an underwater basin using ambient noise tomography. For atmospheric applications, Zhu and Stensrud (2019) used a run of telecommunications fiber and time-reversal migration to track the location of thunder strikes. They also found the DAS signal power were loosely correlated with the reported current power. Currenti et al. (2020) compared DAS recordings of the Etna Volcano (Italy) to traditional broadband and infrasound sensing arrays. They found DAS is able to record both broadband seismic and infrasound sources, at least qualitatively, produced by the volcano, as compared to traditional sensors.

Efforts to use fiber-optic technology to record sound waves date back at least to Cole et al. (1977) and several high-quality, fiber-based microphones have been commercially available for almost a decade (e.g., Bucaro et al., 2005). However, research into

using DAS to construct a *distributed array* of acoustic sensors is relatively recent. Zamarreño et al. (2017) used intensity-based time-domain reflectometry (iODTR) to record sound waves in the audible range on coiled sections of fiber, but their technique only allowed for focusing on one source at a time. Likewise, Masoudi et al. (2014) used phase-based OTDR to detect sound waves in the 200 Hz to 50 kHz frequency range recorded by fiber attached to a rectangular membrane. Liu et al. (2021) used phase-based OTDR with fiber wrapped around 3D-printed solid discs to form an array for locating underwater acoustic sources, but they also demonstrated the method for sound waves transmitted through air. Li et al. (2020) used a coherent OTDR to construct an array of acoustic sensors by wrapping fiber around 3D-printed hollow cylinders, a concept used in the development of acoustic accelerometers (e.g., Pechstedt and Jackson, 1995). Importantly, Li et al. (2020) also explored the cylindrical transducer’s sensitivity dependence on geometric and material property parameters. For the tested configuration, they found a lower Poisson’s ratio, Young’s Modulus, and wall thickness increased the transducer sensitivity, while increasing radius increased sensitivity. They achieved impressive results using distributed microstructured optical fiber (DMOF), but DMOF does require special post-processing and not all commercially available DAS units support it.

The goal of our work is not to develop the best DAS-based microphone possible, but rather to develop “good enough” sensors which can be easily assembled for geophysical and industrial applications with off-the-shelf products. For this reason, we elect to use standard single mode fiber and a lower-cost, commercially available, true-phase DAS interrogator. Using a small speaker, we test the acoustic response to various sound sources of tactical fiber deployed in straight lines on the ground and suspended from the ceiling, as well as tight buffered fiber attached to various common objects, including a Plexiglas sheet, a tire, a loose coil, and a PVC pipe. For the cylinder case, we build on the work of Li et al. (2020) by quantifying signal distortions and effects of varying the length of fiber included on the sensor. Finally, we detail future work to better understand the sensors sensitivity and to improve its response.

2 DATA

For the experiments described below we used a Terra15 Treble true-phase DAS interrogator. The interrogator was configured as shown in Table 3.1. The Treble interrogator is somewhat distinct in that it records in a “velocity” format (i.e., deformation rate) along the fiber rather than strain rate and is less expensive than most phase sensitive DAS units. We used a time-stamped video-recording application running on an cell phone to both document the experiment and record the sound sources, which will serve as an important benchmark against which to compare DAS recordings.

We employed a 12 W programmable speaker to play a variety of sources. The speaker manufacturer reports a frequency range of 90Hz to 20kHz, but does not provide amplitude or phase curves. The source suite included linear and logarithmic sweeps, monotonies (sine-based harmonics), and recordings of rockbursts, a type of failure experienced in underground mines we aim to use our microphones to study in the future.

For the first set of experiments, the fiber array consisted of approximately 200 m of tactical, dual-strand, single mode fiber-optic cable deployed in the basement of the Green Center at the Colorado School of Mines. Two fiber loops were deployed in the hallways, one on the floor and the other fastened to the ceiling with magnetic clips at irregular spacing. In addition to the fiber deployed in the hallway, we also recorded and analyzed data on a few hundred meters of fiber on the spool. We refer to the fiber segments suspended from the ceiling, the fiber laying on the ground, and the fiber on the spool as suspended, ground, and spooled fiber, respectively.

The sensors in the second second experiment consisted of: (1) 40 m of single mode tight buffered (SMTB) fiber wrapped around a 60cm diameter rubber tire, (2) 40 m of SMTB fiber wrapped around a 8 cm diameter, 23 cm long PVC schedule 40 pipe, (3) 20 m of SMTB fiber fastened to the front of a 45 cm by 60 cm Plexiglas sheet, and (4) 20 m of fiber loosely coiled in loop with a diameter of 30 cm.

For the first set of experiments, the suite of sources was played at three locations; two in the hallway and one approximately 100 cm from the spool. For the second experiment, each sensor under test was suspended from the ceiling and the speaker placed 2 m away and oriented toward the sensor. All of the sensors were tested in the basement of the Green Center, with the exception of the tire which was tested at CSM’s Edgar experimental underground mine because it was more practical to suspend a heavy object from the mine ceiling. The sheet was oriented facing the speaker such that the largest surface area is perpendicular to the propagation of the sound waves. The tire was oriented in a similar manner.

Parameter	Experiment 1	Experiment 2
Pulse Length (m)	1.84	0.82
Sampling Width (m)	0.82	0.82
Sampling Rate (Hz)	24,000	40,000
Fiber Type	SM Tactical, SM	Tight Buffered

Table 1. Summary of parameters in the DAS interrogator and fiber setup.

3 METHODS

3.1 Tap Test

For both experiments, we performed the standard “tap test” to orient the fiber (i.e., to map the along-fiber distance reported by the interrogator to physical locations). While this technique worked as expected for the fiber deployed on the ground from Experiment 1, the taping on the suspended fiber was much less centralized in both space and time and a large amount of “ringing” occurred as the perturbed fiber continued to oscillate (see Figure 2). However, vertical stripping is apparent in suspended fiber tap test, which corresponds to the fastening points on the ceiling. Figure 1 shows the fiber locations, designated by each segment’s distance from the interrogator, for both suspended fiber (blue) and ground fiber (red). We found it is better to orient the suspended fiber using the mounting point locations rather than trying to localize the tap itself. For the fiber sensors, the standard tap test worked sufficiently well, but it was also useful to gently scrape the fiber wrapped around the objects to illuminate the sensor fiber location.

3.2 Fiber Aggregation

For each object, the data reported by the DAS interrogator is aggregated in order to form a single stream of data. Calculating the integrated strain rate of the fiber associated with each acoustic sensor is straightforward because the Terra15 interrogator records the along-fiber velocity. Basically, the first channel associated with the sensor is subtracted from the last according to

$$S(t) = \int_{x_1}^{x_2} \dot{\epsilon}(t, x) dx = \dot{X}[t, x_2] - \dot{X}[t, x_1], \tag{1}$$

where $S(t)$ is Sensor recording (proportional to velocity); $\dot{\epsilon}$ is the along fiber strain rate (1/s); \dot{X} is the along fiber velocity (m/s, native format of interrogator); t is time (s); and x_1 and x_2 are the start and end x positions of the acoustic sensor (m).

3.3 Signal Discovery and Alignment

To compare the signal recorded by the sensors for each source, we employ a sliding normalized correlation operator which, in the discrete time domain, takes the following form:

$$cc[i] = \frac{S[i : i + len(J)] \cdot J}{|S[i : i + len(J)]| \cdot |J|}, \tag{2}$$

where i is integer index; cc it the normalized cross correlation; S is the discrete sensor signal found with equation 1; len is the length operator; J is the signal provided to the speaker; and f_2 is the source frequency (+2.5 Hz).

We then find the segment of each recorded signal that aligns to each of the source waveforms by finding the index i that maximizes cc . We note that cc also provides a measure of how well each signal was recorded. However, since there are distortions of the input signal caused by the speaker and path propagation, the signal actually received by the sensors can be quite different. As reference, we currently use the signal recorded by the cell phone, which is co-located with the other sensors.

3.4 Signal-to-Noise Calculations

For the second experiment, we compute the signal-to-noise ratio (SNR) for each of the tested objects and each monotone, which provides a means of comparing frequency-dependant sensitivities. The SNR ratio is determined by calculating a power spectra for each object’s recording of the monotonies and for background noise levels. The sum of the power spectra around the signal source frequency is then divided by the sum of the background noise around over the same frequencies to determine SNR (equation 3):

$$SNR = 10 \log \left(\frac{\sum_{f=f_1}^{f_2} S(f)}{\sum_{f=f_1}^{f_2} B(f)} \right), \tag{3}$$

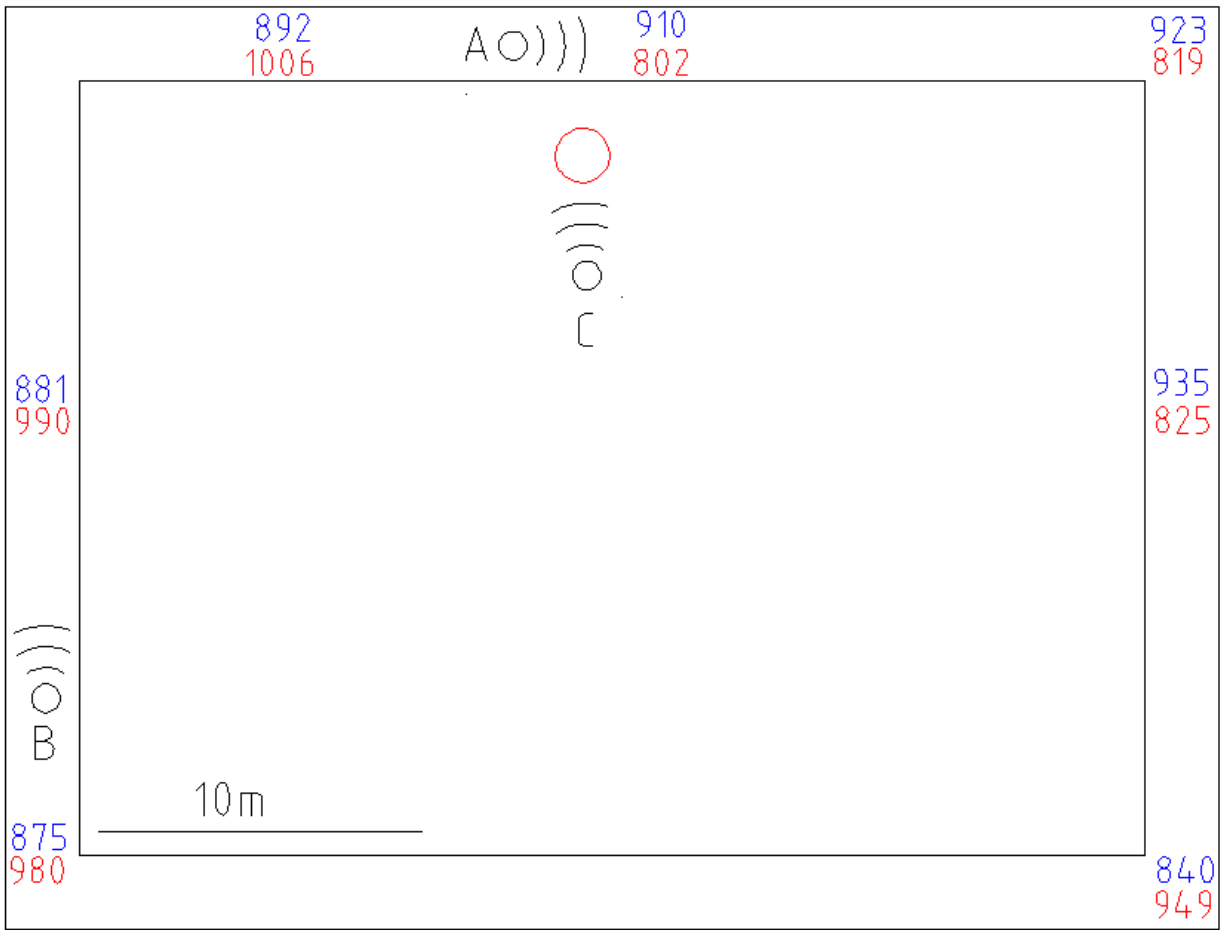


Figure 1. Map of the deployed fiber and sources for experiment 1. Red and blue numbers indicate length along the fiber for the fiber deployed on the floor and ceiling, respectively. Numbers show the location of source initiation and the red circle indicates the location of the fiber spool.

where $S(f)$ is signal power spectra; $B(f)$ is background power spectra; f is frequency (Hz); and frequency limits f_1 and f_2 are $f \pm 2.5$ Hz, respectively.

4 RESULTS

Both the suspended and ground fiber from the first experiment failed to record the acoustic signals to such a quality they were visible in spectrograms. However, the source acquired on the spooled fiber did record the signal (see Figure 3). All of the acoustic sensors recorded some of the sources, but in order to compare each of the frequency-dependent sensitivity we examine the SNR of each sensor to the suite of monotone sources (see Figure 4). Of all the fiber sensors (which does not including the cell phone), the cylinder has the highest SNR to over the largest range of frequencies. The cylinder is only less sensitive than the sheet for $f < 400$ Hz and less sensitive than the tire at $f < 600$ Hz. However, unlike the cylinder, the sensitivity of the sheet and the tire likely have strong dependence on their orientation with regards to the speaker, so the cylinder design may still be desirable for lower-frequency applications.

We also examine the correlation coefficient (equation 2) for a variety of sweeps and rockburst input signals (Table 4). Sweep_1 is a 30 s linear sweep from 100Hz to 300Hz, sweep_2 is a 30 s linear sweep from 100 Hz to 10kHz, and sweep_3 is a 30 s logarithmic sweep from 100Hz to 300Hz. In each case, the phone recorded the best signal, as expected. Of the fiber-based sensors, the cylinder performs best for the broad spectrum sweeps but is outperformed by both the sheet and the tire when the frequencies are limited

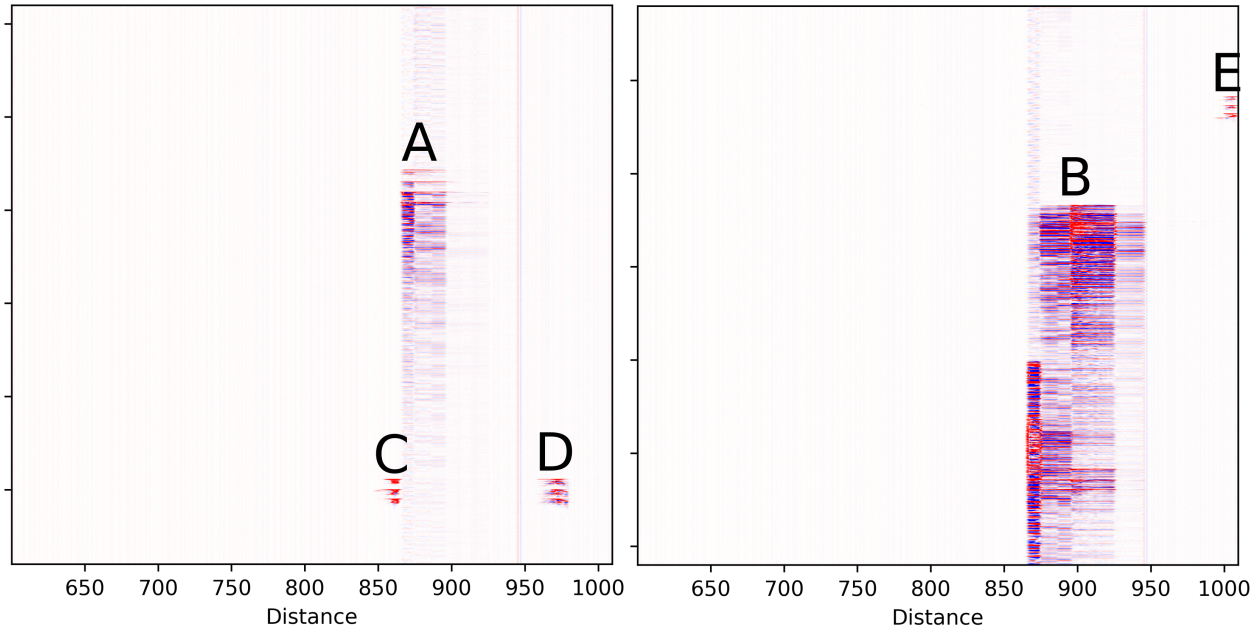


Figure 2. Example tap-test waveforms from Experiment 1. A and B show examples of the tap test performed on suspended sections of cable where A was performed on a fastening point and B was performed in between fastening points. C, D, and E show waveforms for fiber sections on the ground. The x-axis plots distance along the fiber (in m) and the ticks on the y-axis represent 5 s intervals.

	burst_0	burst_1	burst_2	burst_3	sweep_1	sweep_2	sweep_3
coil	0.04	0.05	0.05	0.05	0.01	0.06	0.06
cylinder	0.03	0.06	0.10	0.04	0.03	0.15	0.25
phone	0.32	0.19	0.19	0.30	0.81	0.43	0.50
sheet	0.09	0.07	0.05	0.11	0.20	0.03	0.05
tire	0.07	0.10	0.09	0.14	0.25	0.11	0.15

Table 2. Correlation coefficient for each sensor and source.

to 300 Hz (a predictable result based on the sensitivities shown in Figure 4). For the rockbursts, no single fiber sensor consistently outperformed the others.

5 DISCUSSION

In all cases, the coiled fiber sensor performed worse than any other sensor. This confirms that the material and geometry selected contributed significantly to the sensitivity of the sensor.

5.1 Suspending Fiber

Although the straight, suspended fiber from experiment failed to adequately record acoustic signals, some of the findings in orienting suspended fiber (Figure 2) and the relative increase in background noise levels (Figure 5.1) may be useful for installing quasi-distributed suspended acoustic sensors or for deploying suspended fiber for other measurements, such as monitoring ventilation.

The suspended fiber has significantly higher noise characteristics in all frequency ranges. Figure 5.1 shows the 10% to 90% quantiles of approximately 250 1.0 s smoothed amplitude spectra taken during relatively quiet times during the experiment. The fiber segments plotted include 10 m sections of ground and suspended fiber in front of source A and 10 m of spooled fiber in front of source C (see Figure 1). The noise levels are lowest for the spooled fiber, but the ground fiber has similar characteristics.

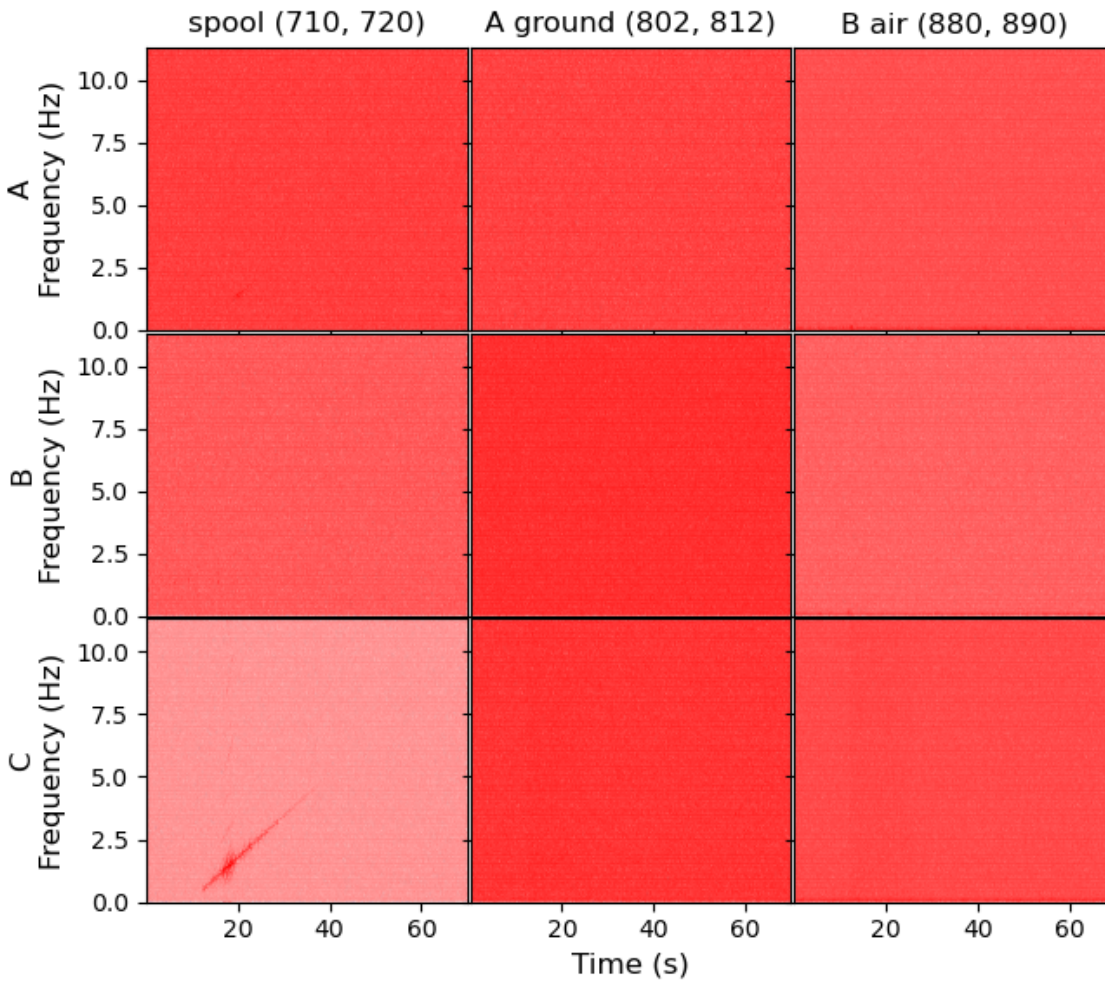


Figure 3. Spectrogram of velocity data of the linear frequency sweeps for various fiber segments and sources from experiment 1. The time slice of the first channel in each segment was subtracted from the other segments to remove the imprinted upstream signal and the last channel was used to generate the spectrogram.

5.2 Fiber Length Dependence

A question of significant practical importance is how much fiber each sensor needs, since minimizing the number of wraps lessens the fabrication burden and frees up more fiber for other sensing. Although the interference patterns of SM fiber introduces more uncertainty than FBG (e.g., Lindsey et al., 2020), when a sufficient number of channels are combined this effect is likely to diminish. Figure 6 shows the SNRs for different lengths fiber wrapped around the cylinder sensor. For the most part, increasing the length of fiber increases SNR approaching some asymptotic limit. Interestingly, however, 30m seems to perform better than 40m. We believe this is due to errors in estimating the starting and ending of the cylinder fiber (with the tap tests) resulting in some of the 40m being off the cylinder.

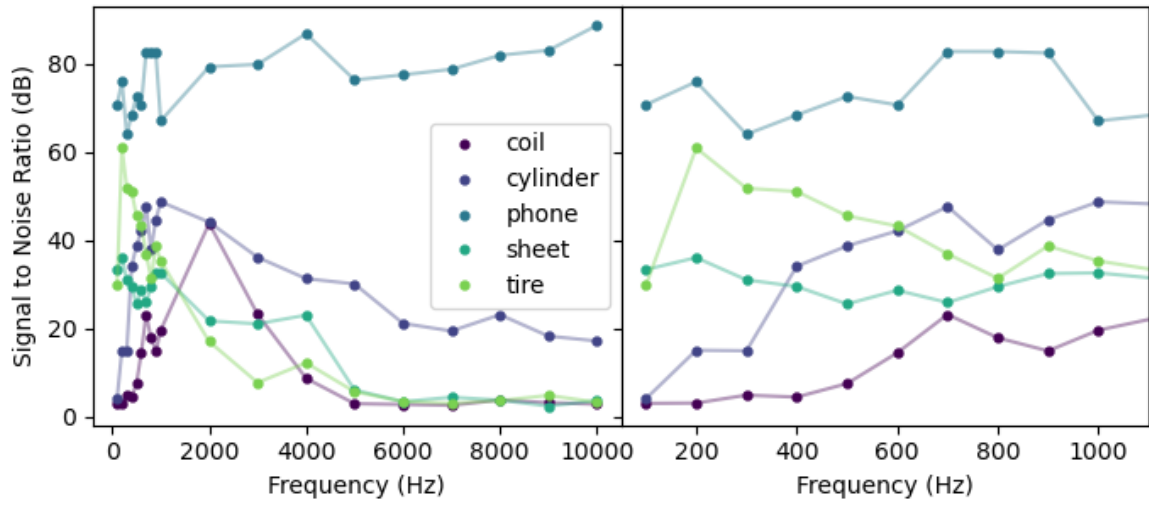


Figure 4. Frequency-dependent SNR for each of the acoustic sensors. Both panels show the same data series; however, the right side zoomed into $f < 1000$ Hz.

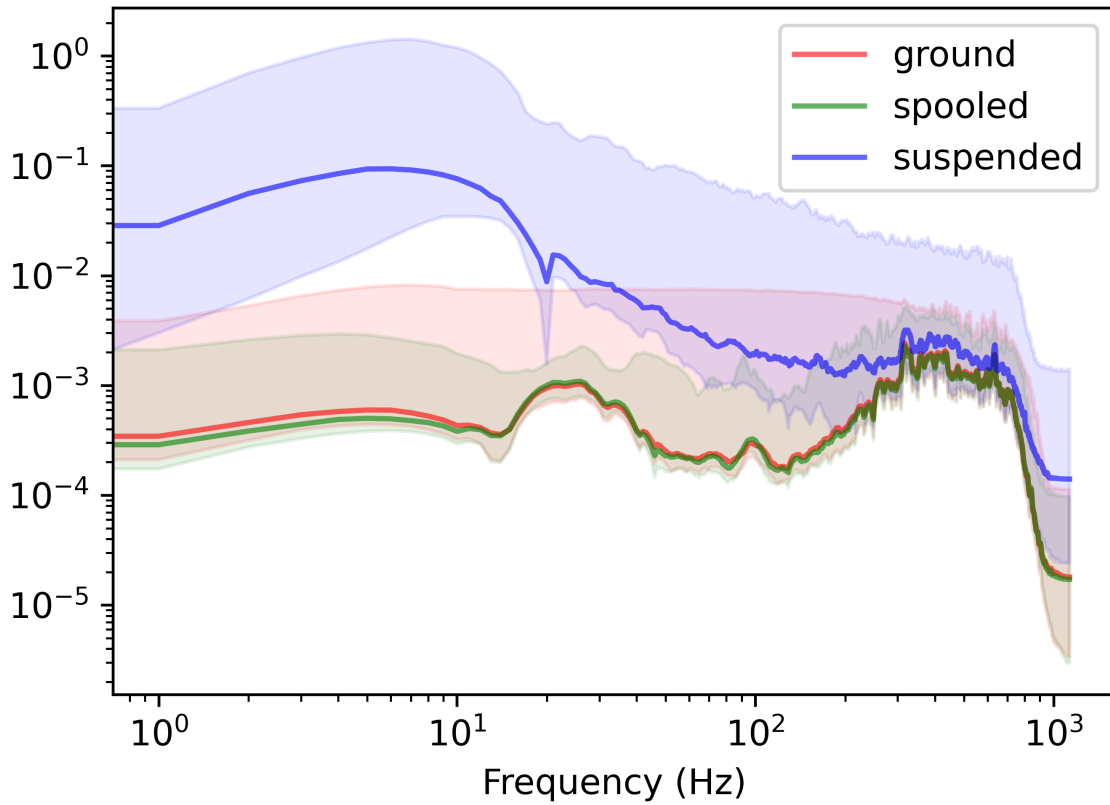


Figure 5. Noise spectra from approximately 250 1-s smoothed amplitude spectra calculated by 10 m lengths of each fiber type. Time windows for amplitude spectra were selected during times the acoustic source was deactivated.

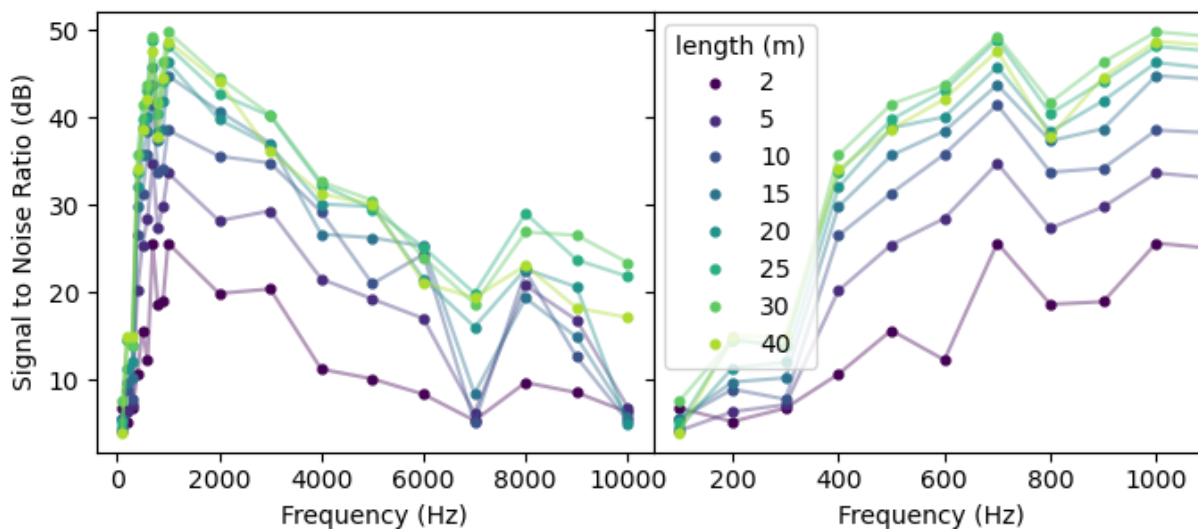


Figure 6. Effects of fiber length included in cylindrical sensor.

5.3 Future Work

Since this work is preliminary, there are several areas we still intended to explore. We will primarily focus on understanding and improving the response of the cylinder sensor as it is the easiest to assemble and deploy, and the optimal signal for a broad range of frequencies.

First, our measurements of SNR and correlation coefficient are somewhat relative. We plan to repeat these experiments for the sensing objects with a colocated, calibrated sensing microphone (rather than the cell phone) to calculate a transfer function which relates DAS measurements to air pressure. Of course, there are additional complexities that need to be accounted for in applying the transfer function to other similar sensors, such as the interrogator settings and along-fiber attenuation which increases with sensor-interrogator distance.

Second, we intend to explore directional effects along the primary axis of the cylinder. From listening to some of the sensor recordings of voices, there appears to be significant variability depending on the angle from the speaker to the cylinder. Qualitatively, it appears the cylinder is most sensitive around 45° , but this needs to be confirmed experimentally.

Third, the modeling results of Li et al. (2020) suggest the geometric and material properties of the cylinder can have significant impacts on the sensitivity; however, due to the need to manage model complexity they did not take into account the effect of the fiber on the cylinder system. In that light, we intend to quantify the response of variably sized cylinders made of different materials and wrapped with different types of SM fiber (e.g., tactical, riser, tight buffered), with particular focus on finding configurations with improved low frequency sensitivity.

Ultimately, our aim is to assemble and demonstrate sensors which broaden the sensing abilities of DAS arrays. For example, in an underground mining environment, a single DAS array could record seismic signals from straight fiber coupled to the rock, changes in ventilation using suspended fiber, acoustic signals related to both rockbursting as well as other mining activities, with the types of sensors described in this paper. As noted by Liu et al. (2018), fiber-optic sensing technology has immense potential to improve operations and safety in underground mines.

6 CONCLUSIONS

We have compared various configurations of fiber for sensing acoustic wave propagation through air. We found a cylinder design has the best performance over a broad frequency range but is deficient in lower frequencies. Although this work is in the beginning stages, we have made progress in developing a simple DAS microphone which can be used in conjunction with traditional DAS arrays for a variety of geophysical and industrial monitoring scenarios.

7 ACKNOWLEDGEMENTS

We thank the National Institute for Occupational Safety and Health (**NIOSH**) and the sponsor companies of the Center for Wave Phenomena for supporting this research.

REFERENCES

- Bucaro, J. A., N. Lagakos, B. H. Houston, J. Jarzynski, and M. Zalalutdinov, 2005, Miniature, high performance, low-cost fiber optic microphone: *J. Acoust. Soc. Am.*, **118**, 1406–1413.
- Cole, J. H., R. L. Johnson, and P. G. Bhuta, 1977, Fiber-optic detection of sound: *J. Acoust. Soc. Am.*, **62**, 1136–1138.
- Currenti, G., P. Jousset, A. Chalari, L. Zuccarello, R. Napoli, T. Reinsch, and C. Krawczyk, 2020, Fibre optic Distributed Acoustic Sensing of volcanic events at Mt Etna: ui.adsabs.harvard.edu, 11641.
- Karrenbach, M., A. Ridge, S. Cole, K. Boone, J. Rich, K. Silver, and D. Langton, 2017, DAS microseismic monitoring and integration with strain measurements in hydraulic fracture profiling: Presented at the Proceedings of the 5th Unconventional Resources Technology Conference, American Association of Petroleum Geologists.
- Li, H., Q. Sun, T. Liu, C. Fan, T. He, Z. Yan, D. Liu, and P. P. Shum, 2020, Ultra-High sensitive Quasi-Distributed acoustic sensor based on coherent OTDR and cylindrical transducer: *J. Lightwave Technol.*, **38**, 929–938.
- Lindsey, N. J., E. R. Martin, D. S. Dreger, B. Freifeld, S. Cole, S. R. James, B. L. Biondi, and J. B. Ajo-Franklin, 2017, Fiber-optic network observations of earthquake wavefields: *Geophys. Res. Lett.*, **44**, 11–792.
- Lindsey, N. J., H. Rademacher, and J. B. Ajo-Franklin, 2020, On the broadband instrument response of fiber-optic DAS arrays: *J. Geophys. Res. [Solid Earth]*, **125**.
- Lior, I., D. E. Mercerat, D. Rivet, A. Sladen, and J.-P. Ampuero, 2021, Imaging an underwater basin and its resonance modes using optical fiber distributed acoustic sensing: *EarthArXiv*, <https://doi.org/10.31223/X5XK8P>.
- Liu, T., Y. Wei, G. Song, B. Hu, L. Li, G. Jin, J. Wang, Y. Li, C. Song, Z. Shi, L. Zhao, J. Hu, W. Zhao, M. Hou, R. Li, and J. Wang, 2018, Fibre optic sensors for coal mine hazard detection: *Measurement*, **124**, 211–223.
- Liu, Z., L. Zhang, H. Wei, Z. Xiao, Z. Qiu, R. Sun, F. Pang, and T. Wang, 2021, Underwater acoustic source localization based on phase-sensitive optical time domain reflectometry: *Opt. Express*, **29**, 12880–12892.
- Masoudi, A., M. Belal, and T. P. Newson, 2014, Distributed optical fibre audible frequency sensor: 23rd International Conference on Optical Fibre Sensors, SPIE, 537–540.
- Molenaar, M. M., and B. E. Cox, 2013, Field cases of hydraulic fracture stimulation diagnostics using fiber optic distributed acoustic sensing (DAS) measurements and analyses: Presented at the Spe unconventional gas conference and exhibition, onepetro.org.
- Pechstedt, R. D., and D. A. Jackson, 1995, Design of a compliant-cylinder-type fiber-optic accelerometer: theory and experiment: *Appl. Opt.*, **34**, 3009–3017.
- Spica, Z. J., M. Perton, E. R. Martin, G. C. Beroza, and B. Biondi, 2020, Urban seismic site characterization by Fiber-Optic seismology: *J. Geophys. Res. [Solid Earth]*, **125**, 1251.
- Zamarreño, C. R., C. Martelli, R. Daciuk, G. Dutra, U. J. Dreyer, J. C. Cardozo Da Silva, I. R. Matias, and F. J. Arregui, 2017, Distributed optical fiber microphone: 2017 IEEE SENSORS, ieeexplore.ieee.org, 1–3.
- Zhu, T., and D. J. Stensrud, 2019, Characterizing thunder-induced ground motions using fiber-optic distributed acoustic sensing array: *J. Geophys. Res.*, **124**, 12810–12823.
- Zuo, M., X. Tu, S. Yang, H. Fang, X. Wen, and F. Qu, 2021, Channel distribution and noise characteristics of distributed acoustic sensing underwater communications: *IEEE Sens. J.*, **21**, 24185–24194.